INTERNATIONAL VIDEO JOURNAL OF ENGINEERING RESEARCH, Vol. , 83–96 (1991)

SPACE–TIME FINITE ELEMENT COMPUTATION OF INCOMPRESSIBLE FLOWS WITH EMPHASIS ON FLOWS INVOLVING OSCILLATING CYLINDERS

S. MITTAL, A. RATNER, D. HASTREITER AND T. E. TEZDUYAR

Department of Aerospace Engineering and Mechanics, Army High-Performance Computing Research Center and Minnesota Supercomputer Institute, University of Minnesota, 1200 Washington Avenue South, Minneapolis, MN 55455, U.S.A.

SUMMARY

In this article, the stabilized space–time finite element formulation of incompressible flows, including those involving moving boundaries and interfaces, is reviewed, and results are presented for certain unsteady flows past a circular cylinder. One of the cases studied is flow past a cylinder which is forced to oscillate in the horizontal direction. The case in which the cylinder is mounted on a flexible support and allowed to oscillate in the vertical direction is also studied. In the latter case the motion of the cylinder needs to be determined as part of the solution. Efficient iteration techniques are employed to solve the equation systems resulting from the space–time finite element discretization of the problem.

1. INTRODUCTION

The space–time formulation is used in conjunction with GLS (Galerkin/least-squares) stabilization. GLS stabilization prevents numerical oscillations that might be produced by the presence of dominant advection terms in the governing equations or by not using an acceptable combination of interpolation functions to represent the velocity and pressure fields. In this kind of stabilization, a series of stabilizing terms is added to the Galerkin formulation of the problem. These terms can be obtained by minimizing the sum of the squared residual of the momentum equation integrated over each element domain. The GLS stabilization leads to a consistent formulation, in the sense that an exact solution still satisfies the stabilized formulation. Consequently, it introduces minimal excess diffusion, and therefore results in solutions with minimal loss of accuracy.

The space–time finite element formulation with GLS stabilization has recently been used for various problems with fixed spatial domains. These authors are most familiar with the work of Hughes *et al.*,[1] Hughes and Hulbert,[2] Shakib,[3] and Hansbo and Szepessy.[4] The basics of the space–time formulation, its implementation, and the associated stability and accuracy analysis can be found in these references.

In the space–time formulation, finite element discretization is applied not only spatially but also temporally. Consequently, the deformation of the spatial domain is taken into account automatically. This feature of the stabilized space–time formulation was first pointed out and implemented by Tezduyar *et al.*[5,6] They introduced the Deforming-Spatial-Domain/Space–Time (DSD/ST) procedure and applied it to several unsteady incompressible flow problems involving moving boundaries and interfaces, such as free-surface flows, liquid

1052–9268/91/020083–14$07.00

Received 2 September 1991
Revised 8 October 1991

drops, two-liquid flows and flows with drifting cylinders. In the DSD/ST procedure the frequency of remeshing is minimized. Here we define remeshing as the process of generating a new mesh, and projecting the solution from the old mesh to the new one. Since remeshing, in general, involves projection errors, minimizing the frequency of remeshing results in minimizing the projection errors. Furthermore, minimizing the frequency of remeshing increases the massive parallelization potential of the computations.

It is important to realize that the finite element interpolation functions are discontinuous in time so that the fully discrete equations are solved one space–time slab at a time, and this makes the computations feasible. Still, the computational cost associated with the space–time finite element formulations using piecewise linear functions in time is quite heavy. For large-scale problems it becomes imperative to employ efficient iteration methods to reduce the cost involved. This was achieved by Liou and Tezduyar[7] by using the generalized minimal residual (GMRES)[8] iteration algorithm with the clustered element-by-element (CEBE) preconditioners.

The CEBE method is a generalized version of the standard element-by-element method.[9,10] In this technique the elements are partitioned into clusters of elements, with a desired number of elements in each cluster, and the iterations are performed in a cluster-by-cluster fashion. The number of clusters should be viewed as an optimization parameter to minimize the computational cost (both memory and CPU time). By specifying the number of clusters, one can select an algorithm anywhere in the spectrum of algorithms ranging from the direct solution technique (when the number of clusters is one) to the standard element-by-element method (when the number of clusters is the same as the number of elements).

The numerical examples considered here consist of certain unsteady flows past a circular cylinder. First, flow past a fixed circular cylinder at Reynolds number (based on the free-stream velocity) 100 is solved. Then, at the same Reynolds number, the cylinder is subjected to forced horizontal oscillations; this leads to a symmetric mode of vortex shedding. The final case studied involves flow past a circular cylinder that is mounted on flexible supports and is free to respond to the fluid forces in the vertical direction; the Reynolds number for this simulation is 324.

2. GOVERNING EQUATIONS

Let $\Omega_t \in R^{n_{sd}}$ be the spatial domain at time $t \in (0, T)$, where n_{sd} is the number of space dimensions. Let Γ_t denote the boundary of Ω_t. We consider the following velocity–pressure formulation of the Navier–Stokes equations governing unsteady incompressible flows:

$$\rho\left(\frac{\partial \mathbf{u}}{\partial t} + \mathbf{u}\cdot\nabla\mathbf{u}\right) - \nabla\cdot\sigma = \mathbf{0} \qquad \text{on } \Omega_t \ \forall t \in (0, T) \tag{1}$$

$$\nabla\cdot\mathbf{u} = 0 \qquad \text{on } \Omega_t \ \forall t \in (0,T) \tag{2}$$

where ρ and $\mathbf{u}$ are the density and velocity, and σ is the stress tensor given as

$$\sigma(p,\mathbf{u}) = -p\mathbf{I} + 2\mu\varepsilon(\mathbf{u}) \tag{3}$$

with

$$\varepsilon(\mathbf{u}) = \tfrac{1}{2}(\nabla\mathbf{u} + (\nabla\mathbf{u})^T) \tag{4}$$

here p and μ are the pressure and the dynamic viscosity, and $\mathbf{I}$ is the identity tensor. The part of the boundary at which the velocity is assumed to be specified is denoted by $(\Gamma_t)_g$:

$$\mathbf{u} = \mathbf{g} \qquad \text{on } (\Gamma_t)_g \ \forall t \in (0, T) \tag{5}$$

The 'natural' boundary conditions associated with (1) are the conditions on the stress components, and these are the conditions assumed to be imposed at the remaining part of the boundary:

$$\mathbf{n}\cdot\sigma = \mathbf{h} \qquad \text{on } (\Gamma_t)_{\mathbf{h}} \ \forall t \in (0, T) \tag{6}$$

The homogeneous version of (6), which corresponds to the 'traction-free' (i.e., zero normal and shear stress) conditions, is often imposed at the outflow boundaries. As initial condition, a divergence-free velocity field $\mathbf{u}_0(\mathbf{x})$ is specified over the domain Ω_t at $t = 0$:

$$\mathbf{u}(\mathbf{x}, 0) = \mathbf{u}_0(\mathbf{x}) \qquad \text{on } \Omega_0 \tag{7}$$

3. STABILIZED SPACE–TIME FINITE ELEMENT FORMULATION

In the space–time finite element formulation, the time interval $(0, T)$ is partitioned into subintervals $I_n = (t_n, t_{n+1})$, where t_n and t_{n+1} belong to an ordered series of time levels $0 = t_0 < t_1 < \ldots < t_N = T$. It was first shown by Tezduyar *et al.*[5,6] that the stabilized space–time finite element formulation can be effectively applied to fluid dynamics computations involving moving boundaries and interfaces. In this formulation the spatial domains at various time levels are allowed to vary. We let $\Omega_n = \Omega_{t_n}$ and $\Gamma_n = \Gamma_{t_n}$, and define the space–time slab Q_n as the space–time domain enclosed by the surfaces Ω_n, Ω_{n+1} and P_n (see Figure 1). Here P_n, the lateral surface of Q_n, is the surface described by the boundary Γ, as t traverses I_n. Similar to the way it was represented by equations (5) and (6), P_n is decomposed into $(P_n)_{\mathbf{g}}$ and $(P_n)_{\mathbf{h}}$ with respect to the type of boundary condition being imposed.

Finite element discretization of a space–time slab Q_n is achieved by dividing it into elements Q_n^e, $e = 1, 2, \ldots, (n_{el})_n$, where $(n_{el})_n$ is the number of elements in the space–time slab Q_n. Associated with this discretization, for each space–time slab we define the following finite element interpolation function spaces for the velocity and pressure:

$$(S_{\mathbf{u}}^h)_n = \{\mathbf{u}^h \mid \mathbf{u}^h \in [H^{1h}(Q_n)]^{n_{sd}},\ \mathbf{u}^h = \mathbf{g}^h \text{ on } (P_n)_{\mathbf{g}}\} \tag{8}$$

$$(V_{\mathbf{u}}^h)_n = \{\mathbf{w}^h \mid \mathbf{w}^h \in [H^{1h}(Q_n)]^{n_{sd}},\ \mathbf{w}^h = \mathbf{0} \text{ on } (P_n)_{\mathbf{g}}\} \tag{9}$$

$$(S_p^h)_n = (V_p^h)_n = \{q^h \mid q^h \in H^{1h}(Q_n)\} \tag{10}$$

Here $H^{1h}(Q_n)$ represents the finite-dimensional function space over the space–time slab Q_n. This space is formed by using, over the parent (element) domains, first-order polynomials in space and time. It is also possible to use zeroth-order polynomials in time. In either case, globally, the interpolation functions are continuous in space but discontinuous in time.

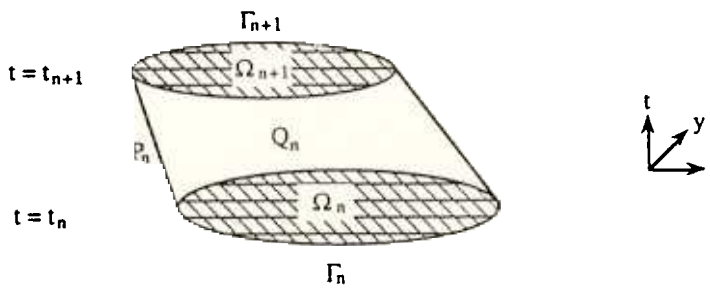

Figure 1. Space-time slab for the DSD/ST formation

The space–time formulation of (1)–(7) can be written as follows: start with

$$(\mathbf{u}^h)_0^- = (\mathbf{u}_0)^h; \tag{11}$$

sequentially for $Q_1, Q_2, \ldots, Q_{N-1}$, given $(\mathbf{u}^h)_n^-$, find $\mathbf{u}^h \in (S_{\mathbf{u}}^h)_n$ and $p^h \in (S_p^h)_n$, such that

$$\forall \mathbf{w}^h \in (V_{\mathbf{u}}^h)_n \quad \text{and} \quad \forall q^h \in (V_p^h)_n$$

$$\int_{Q_n} \mathbf{w}^h \cdot \rho\left(\frac{\partial \mathbf{u}^h}{\partial t} + \mathbf{u}^h \cdot \nabla \mathbf{u}^h\right) \mathrm{d}Q + \int_{Q_n} \varepsilon(\mathbf{w}^h) : \sigma(p^h, \mathbf{u}^h)\, \mathrm{d}Q$$

$$- \int_{(P_n)_h} \mathbf{w}^h \cdot \mathbf{h}\, \mathrm{d}P + \int_{Q_n} q^h \rho \nabla \cdot \mathbf{u}^h\, \mathrm{d}Q + \int_{\Omega} (\mathbf{w}^h)_n^+ \cdot \rho((\mathbf{u}^h)_n^+ - (\mathbf{u}^h)_n^-)\, \mathrm{d}\Omega$$

$$+ \sum_{e=1}^{(n_{el})_n} \int_{Q_n^e} \tau\left[\rho\left(\frac{\partial \mathbf{w}^h}{\partial t} + \mathbf{u}^h \cdot \nabla \mathbf{w}^h\right) - \nabla \cdot \sigma(q^h, \mathbf{w}^h)\right]$$

$$\cdot \left[\rho\left(\frac{\partial \mathbf{u}^h}{\partial t} + \mathbf{u}^h \cdot \nabla \mathbf{u}^h\right) - \nabla \cdot \sigma(p^h, \mathbf{u}^h)\right] \mathrm{d}Q = 0$$

In the variational formulation given by (12), the following notation is being used:

$$(\mathbf{u}^h)_n^{\pm} = \lim_{\delta \to 0} \mathbf{u}^h(t_n \pm \delta)$$

$$\int_{Q_n} (\ldots)\, \mathrm{d}Q = \int_{I_n} \int_{\Omega} (\ldots)\, \mathrm{d}\Omega\, \mathrm{d}t \tag{14}$$

$$\int_{P_n} (\ldots)\, \mathrm{d}P = \int_{I_n} \int_{\Gamma} (\ldots)\, \mathrm{d}\Gamma\, \mathrm{d}t \tag{15}$$

Remark 1. If we were in a standard finite element formulation, rather than a space–time one, the Galerkin formulation of (1)–(7) would have consisted of the first four integrals (their spatial versions of course) appearing in equation (12). In the space–time formulation, because the interpolation functions are discontinuous in time, the fifth integral in equation (12) enforces, weakly, the continuity of the velocity in time. The remaining series of integrals in equation (12) consist of the least-squares terms added to the Galerkin variational formulation to assure the numerical stability of the computations. The coefficient τ determines the weight of such added terms. For the definition of τ see Tezduyar *et al.*[5]

Remark 2. This kind of stabilization of the Galerkin formulation is referred to as the Galerkin/least-squares (GLS) procedure, and can be considered as a generalization of the stabilization based on the streamline-upwind/Petrov–Galerkin (SUPG) and the pressure-stabilizing/Petrov–Galerkin (PSPG) procedure employed for incompressible flows.[11] It is with such stabilization procedures that it is possible to use elements which have equal-order interpolation functions for velocity and pressure, and which are otherwise unstable.

Remark 3. It is important to realize that the stabilizing terms added involve the momentum equation as a factor. Therefore, despite these additional terms, an exact solution is still admissable for the variational formulation given by equation (12).

Remark 4. Because the finite element interpolation functions are discontinuous in time, the fully discrete equations can be solved one space–time slab at a time. Still, the memory needed for the global matrices involved in this method is quite substantial. For example, in two dimensions, the memory needed for space–time formulation (with interpolation functions

which are piecewise linear in time) of a problem is approximately four times more compared to using the finite element method only for spatial discretization. However, iteration methods can be employed to substantially reduce the cost involved in solving the linear equation systems arising from the space–time finite element discretization (see Section 4).

Remark 5. In the DSD/ST procedure, to facilitate the motion of free-surfaces, interfaces and solid boundaries, we need to move the boundary nodes with the normal component of the velocity at those nodes. Except for this restriction, we have the freedom to move all the nodes any way we would like to. With this freedom, we can move the mesh in such a way that we only need to remesh when it becomes necessary to do so to prevent unacceptable degrees of mesh distortion and potential entanglements. By minimizing the frequency of remeshing we minimize the projection errors expected to be introduced by remeshing. In fact, for some computations, as a byproduct of moving the mesh, we may be able to get a limited degree of automatic mesh refinement, again with minimal projection errors. For example, a mesh moving scheme suitable for a single cylinder drifting in a bounded flow domain is described by Tezduyar *et al.*[6] We use the same mesh moving scheme for all the results presented here.

4. CLUSTERED ELEMENT-BY-ELEMENT (CEBE) METHOD

It was pointed out in Remark 4 that the memory needed for the global matrices involved in the space–time method is quite substantial. It was shown by Liou and Tezduyar[7] that the clustered element-by-element (CEBE) preconditioners, together with the generalized minimal residual (GMRES) method[8] can be effectively used to reduce the associated cost significantly. In this section we review the clustered element-by-element method.

After linearization of the fully discretized equations, the following system needs to be solved for the nodal values of the unknowns:

$$\mathbf{A}\mathbf{x} = \mathbf{b}$$

We rewrite (16) in a scaled form

$$\tilde{\mathbf{A}}\,\tilde{\mathbf{x}} = \tilde{\mathbf{b}}$$

where

$$\tilde{\mathbf{A}} = \mathbf{W}^{-1/2}\,\mathbf{A}\mathbf{W}^{-1/2}$$

$$\tilde{\mathbf{x}} = \mathbf{W}^{1/2}\mathbf{x} \tag{19}$$

$$\tilde{\mathbf{b}} = \mathbf{W}^{-1/2}\mathbf{b} \tag{20}$$

The scaling matrix $\mathbf{W}$ is defined as

$$\mathbf{W} = \operatorname{diag} \mathbf{A} \tag{21}$$

With this definition of $\mathbf{W}$, diag $\tilde{\mathbf{A}}$ becomes an indentity matrix.

For the formulations presented in this article, the matrix $\mathbf{A}$ is not in general symmetric and positive-definite. Therefore, the proposed CEBE preconditioner will be used in conjunction with the GMRES method; an outline of the GMRES method used is given below.

Step 0. Set the iteration counter $m = 0$, and start with an initial guess $\tilde{\mathbf{x}}_0$:

Step i. Calculate the residual scaled with the preconditioner matrix $\tilde{\mathbf{P}}$

$$\tilde{\mathbf{r}}_m = \tilde{\mathbf{P}}^{-1}(\tilde{\mathbf{A}}\tilde{\mathbf{x}}_m - \tilde{\mathbf{b}}) \tag{22}$$

Step ii. Construct the Krylov vector space:

$$\mathbf{e}^{(1)} = \tilde{\mathbf{r}}_m / \| \tilde{\mathbf{r}}_m \| \tag{23}$$

$$\mathbf{f}^{(j)} = \tilde{\mathbf{P}}^{-1}\tilde{\mathbf{A}}\,\mathbf{e}^{(j-1)} - \sum_{i=1}^{j-1} (\tilde{\mathbf{P}}^{-1}\tilde{\mathbf{A}}\mathbf{e}^{(j-1)}, \mathbf{e}^{(i)})\mathbf{e}^{(i)}, \quad 2 \leqslant \mathrm{j} \leqslant k \tag{24}$$

$$\mathbf{e}^{(j)} = \mathbf{f}^{(j)} / \|\mathbf{f}^{(j)}\| \tag{25}$$

where k is the dimension of the Krylov space and $\mathbf{e}^{(i)}$, $i = 1, 2, \ldots, k$, are the basis vectors.

Step iii. Update the unknown vector:

$$\tilde{\mathbf{x}}_{m+1} = \tilde{\mathbf{x}}_m + \sum_{j=1}^{k} s_j \mathbf{e}^{(j)}$$

where $\mathbf{s} = \{s_j\}$ is the solution of the equation system

$$\mathbf{Q}\mathbf{s} = \mathbf{z}$$

with

$$\mathbf{Q} = [(\tilde{\mathbf{P}}^{-1}\tilde{\mathbf{A}}\mathbf{e}^{(i)}, \tilde{\mathbf{P}}^{-1}\tilde{\mathbf{A}}\mathbf{e}^{(j)})] \qquad 1 \leqslant \mathrm{i}, \mathrm{j} \leqslant \mathrm{k} \tag{28}$$

$$\mathbf{z} = \{(\tilde{\mathbf{P}}^{-1}\tilde{\mathbf{A}}\,\mathbf{e}^{(i)}, -\tilde{\mathbf{r}}_m)\} \qquad \leqslant \mathrm{i} \leqslant \mathrm{k}$$

Step iv. For next iteration, set $m \leftarrow m + 1$ and go to step *i*:
The iterations continue until $\| \tilde{\mathbf{r}}_m \|$ falls below a predetermined value. It should be noted that the matrix $\mathbf{Q}$ is symmetric and positive-definite.

Remark 6. The convergence rate of this algorithm depends on the condition number of the matrix $\tilde{\mathbf{P}}^{-1}\tilde{\mathbf{A}}$. Therefore one would like to select a preconditioner that involves minimal inversion cost, and provides, within cost limitations, an optimal representation of $\tilde{\mathbf{A}}$.

In the CEBE method, the set of elements ε is partitioned into clusters of elements ε_J, $J = 1, 2, \ldots, N_{\mathrm{cl}}$, where N_{cl} is the number of the clusters. The global matrix $\tilde{\mathbf{A}}_J$ associated with the cluster J is defined as

$$\tilde{\mathbf{A}}_J = \sum_{e \in \varepsilon_J} \tilde{\mathbf{A}}^e$$

where $\tilde{\mathbf{A}}^e$ is the element level matrix associated with element e.

The matrix $\tilde{\mathbf{A}}$ can then be expressed as

$$\tilde{\mathbf{A}} = \mathbf{I} + \sum_{J=1}^{N_{\mathrm{cl}}} \tilde{\mathbf{B}}_J$$

where

$$\tilde{\mathbf{B}}_J = \tilde{\mathbf{A}}_J - \tilde{\mathbf{W}}_J \quad J = 1, 2, \ldots, N_{\mathrm{cl}} \tag{32}$$

The CEBE preconditioning is based on the approximation of (31) by a sequential product of cluster level matrices. The Crout CEBE preconditioner is defined as

$$\tilde{\mathbf{P}} = \prod_{J=1}^{N_{\mathrm{cl}}} \hat{\mathbf{L}}_J \prod_{J=N_{\mathrm{cl}}}^{1} \hat{\mathbf{U}}_J \tag{33}$$

where $\hat{\mathbf{L}}_J$ and $\hat{\mathbf{U}}_J$ are the matrices resulting from the following Crout factorization:

$$(\mathbf{I} + \tilde{\mathbf{B}}_J) = \hat{\mathbf{L}}_J \hat{\mathbf{U}}_J, \quad J = 1, 2, \ldots, N_{\mathrm{cl}} \tag{34}$$

Remark 7. The convergence of the algorithm depends on the numbering of the clusters but not on the numbering of the elements within each cluster. By treating each cluster as a super-element, we can identify the CEBE procedure as a generalization of the standard element-by-element method.

Remark 8. We have the option of storing the cluster matrices and their inverses, or recomputing them as they are needed.

Remark 9. The method is highly vectorizable and parallelizable.

5. NUMERICAL EXAMPLES: UNSTEADY FLOWS PAST A CIRCULAR CYLINDER

All solutions presented here were obtained with linear-in-time interpolation functions. In all cases, the computational values for the cylinder radius and the free-stream velocity are, respectively, 1·0 and 0·125; a time step of 1·0 is used for the computations. The dimensions of the computational domain, normalized by the cylinder radius, are 61·0 and 32·0 in the flow and cross-flow directions, respectively. The mesh employed consists of 4060 elements and 4209 nodes. Symmetry conditions are imposed at the upper and lower computational boundaries, and the traction-free condition is imposed at the outflow boundary. The periodic solution is obtained by introducing a short term perturbation to the symmetric solution. For all computations, we use the CEBE iteration method to solve the resulting equation system. At each time step about 25,000 equations are solved simultaneously. We chose a Krylov vector space of dimension 25 and an average cluster size of 23 elements. For this set of problems, the CEBE technique takes less then one-sixth the CPU time and less than one-third the storage needed by the direct method. The nodal values of the stationary stream function (normalized with the free-stream velocity) and vorticity are obtained by the least-squares interpolation. All the flow-field pictures shown in this paper display the part of the domain enclosed by a rectangular region, with the lower left and upper right co-ordinates (13, 10) and (43, 22) respectively, relative to the lower left corner of the domain.

The data from the solution for the flow field involving oscillating cylinders was used to produce a set of animations to understand these phenomena better. For each of the cases, there are two parts to the animations: one showing the vorticity field and the other showing the stationary stream function. In all the animations, the global flow field is shown at the top half of the screen. The lower half of the screen displays (from left to right) a close-up of the cylinder, the time evolution of the data related to the cylinder, and the color map employed.

5.1. Fixed cylinder at Reynolds number 100

In this problem the cylinder location is fixed at (16, 16) relative to the lower left corner of the domain. Figure 2 shows time history of the lift, drag and torque coefficients for the fixed cylinder. The Strouhal number obtained is 0·167. The difference between this value and the ones reported by Tezduyar et al.,[11] computed with different formulations and on a finer mesh, is less than 2%. Plates I and II show a sequence of frames for the vorticity and stationary stream function during one period of the lift coefficient. In both plates, the first, third and last frames correspond to zero lift coefficient; the second and fourth frames correspond to the trough and crest of the lift coefficient, respectively. As expected, in each of the figures, the first

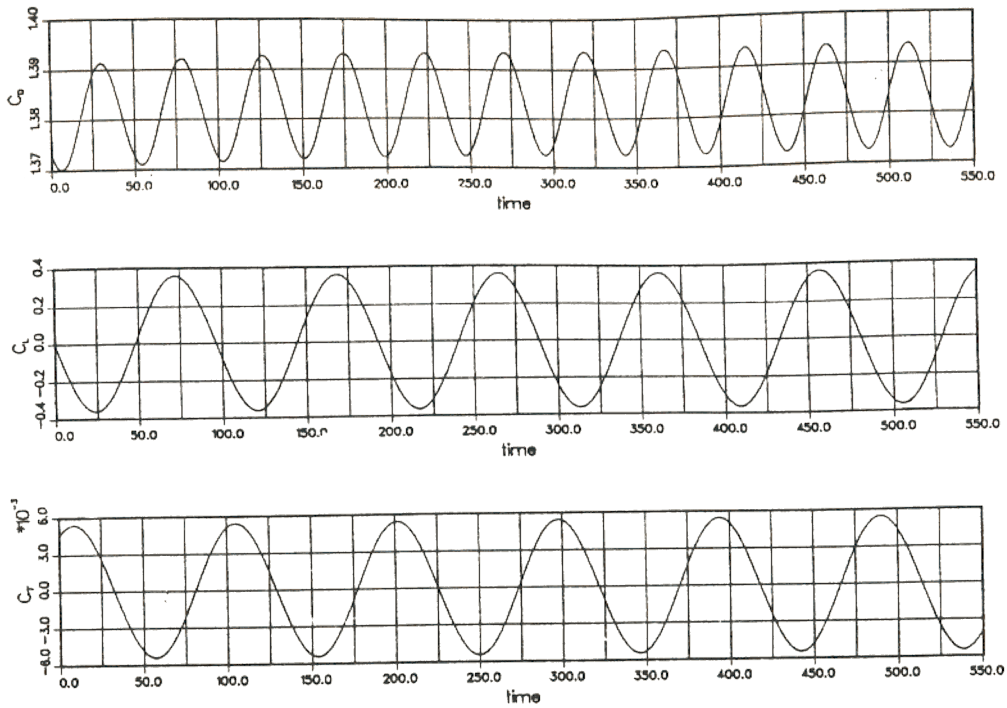

Figure 2. Flow past a fixed cylinder at Re = 100: time history of the lift, drag and torque coefficients

the figures, the first and the last frames are very similar, while the first and third and the second and fourth frames are mirror images of each other.

5.2. *Cylinder with forced horizontal oscillations at Reynolds number 100*

It is well known that at Reynolds number 100, the flow past a fixed circular cylinder leads to classical asymmetrical vortex shedding. In such a case the lift and torque coefficients oscillate with a frequency corresponding to the related Strouhal number, while the drag oscillates with twice that frequency.

The case in which the cylinder is subjected to forced horizontal oscillations shows some very interesting features. Depending on the amplitude and the frequency (f_f) of the forced oscillations of the cylinder, two modes of vortex shedding are possible. This phenomenon of vortex-induced oscillations has been discussed in review papers by King[12] and Sarpkaya.[13] Oscillations with a low reduced frequency ($F_f = 2f_f a/U_\infty$, where a is the radius of the cylinder and U_∞ is the free-stream velocity) lead to asymmetric modes of vortex shedding. For higher values of F_f, on the other hand, symmetric vortex shedding is observed. However, such a symmetric arrangement of vortices is unstable, and consequently the vortices coalesce and eventually become asymmetrical downstream.

We simulate the flow with symmetrical shedding by forcing the cylinder to oscillate horizontally with the following prescribed displacement (normalized by the cylinder radius):

$$X = 1 - \cos(\omega_f t) \tag{35}$$

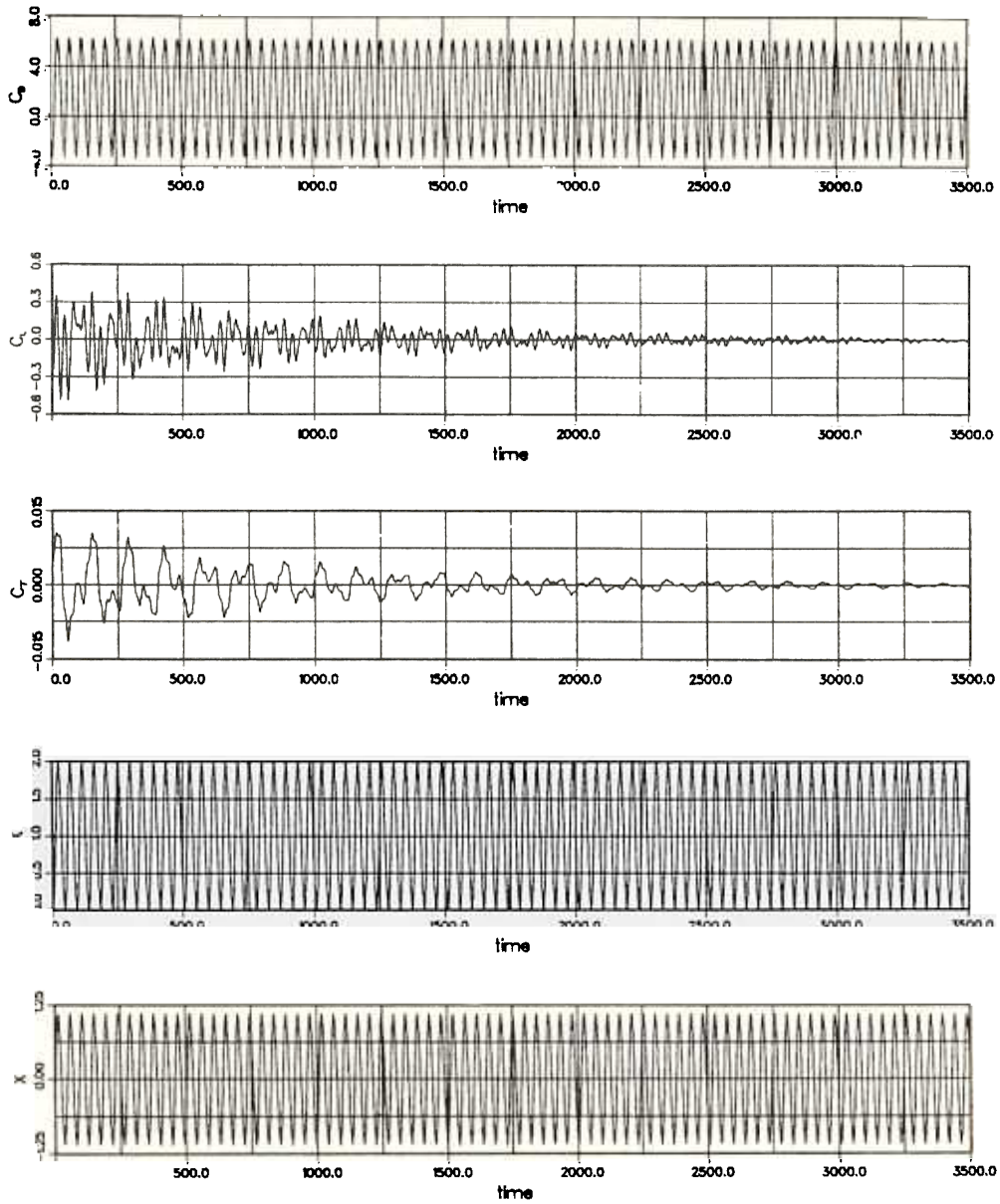

Figure 3. Flow past a horizontally oscillating cylinder at Re = 100: time history of the lift, drag and torque coefficients and the normalized displacement and velocity of the cylinder

where $\omega_f = 2\pi f_f$. For this case, the value of f_f corresponds to a reduced frequency of 0·35. The initial condition for this simulation is prescribed as the unsteady solution for flow past a fixed cylinder at Re = 100 (from the previous example). Figure 3 shows the time history of the drag, lift and torque coefficients and the normalized horizontal displacement and velocity (normalized by the free-stream velocity) of the cylinder. We observe that the drag coefficient for the horizontally oscillating cylinder is significantly larger than that for a fixed cylinder.

Furthermore, the drag coefficient oscillates with a reduced frequency of 0·35 whereas the lift and torque coefficients approach zero. The fact that we start from an asymmetric solution and still obtain a symmetric mode of shedding demonstrates that this mode is a stable one. Plates III and IV show a sequence of frames for the vorticity and stationary stream function during one period of the cylinder motion. In both figures, the first, third and last frames correspond to the mean cylinder location, while the second and fourth frames correspond, respectively, to the left and right extreme positions of the cylinder.

The animations show the transient behaviour of the flow field as the cylinder goes from the asymmetrical vortex shedding mode to the symmetric one. It can be observed that during each period of cylinder motion, two symmetrical pairs of vortices are shed from the cylinder's lower and upper surfaces. One of the pairs of vortices is shed when the cylinder moves in the direction of the flow (the relative Reynolds number for the cylinder is less than 100) while the other is shed when the cylinder motion opposes the free stream flow (the relative Reynolds number for the cylinder is greater than 100). The former pair is much weaker than the latter and diffuses out very quickly.

5.3. Cylinder with vortex-induced vertical oscillations at Reynolds number 324

In the first numerical example we observed that for sufficiently high Reynolds number (>40) flow past a fixed cylinder leads to asymmetric vortex shedding. This causes the cylinder to experience alternating lift force at a frequency corresponding to the Strouhal number for that Reynolds number. Now, if the cylinder is mounted on a flexible support, then under certain conditions it can undergo sustained oscillations with a frequency close to, or coincident with, its natural frequency. These oscillations can alter the vortex shedding mechanism which in turn can change the cylinder response and so on. This leads to a complex non-linear fluid-structure interaction phenomenon and has been the subject of previous research[12–15]. We simulate this phenomenon for a cylinder which is allowed to move only in the vertical direction. The motion of the cylinder is governed by the following equation:

$$\ddot{Y} + 2\pi F_n \zeta \dot{Y} + (\pi F_n)^2 Y = \frac{C_L}{M} \tag{36}$$

Here $\ddot{Y}$, $\dot{Y}$ and Y are, respectively, the normalized vertical acceleration, and the velocity and displacement of the cylinder. The displacement and velocity of the cylinder are normalized by its radius and the free-stream velocity, respectively. M is the non-dimensional mass per unit length of the cylinder, ζ is the structural damping coefficient associated with the system, and C_L denotes the lift coefficient for the cylinder. F_n, the reduced natural frequency of the spring-mass system, is defined as

$$F_n = \frac{2 f_n a}{U_\infty} \tag{37}$$

where f_n is the actual natural frequency of the system. For our problem $F_n = 0{\cdot}204$, $M = 472{\cdot}74$ and $\zeta = 3{\cdot}3 \times 10^{-4}$.

At Reynolds number 324 the reduced natural frequency of the spring mass system and the Strouhal number for flow past a fixed cylinder have very close values. Therefore, we decided to carry out this simulation for Reynolds number 324. The periodic solution for flow past a fixed cylinder at the same Reynolds number is used as the initial condition. Figure 4 shows, for the initial stages of the simulation, the time history of the lift, drag and torque coefficients and the normalized vertical displacement and velocity of the cylinder. We observe that the

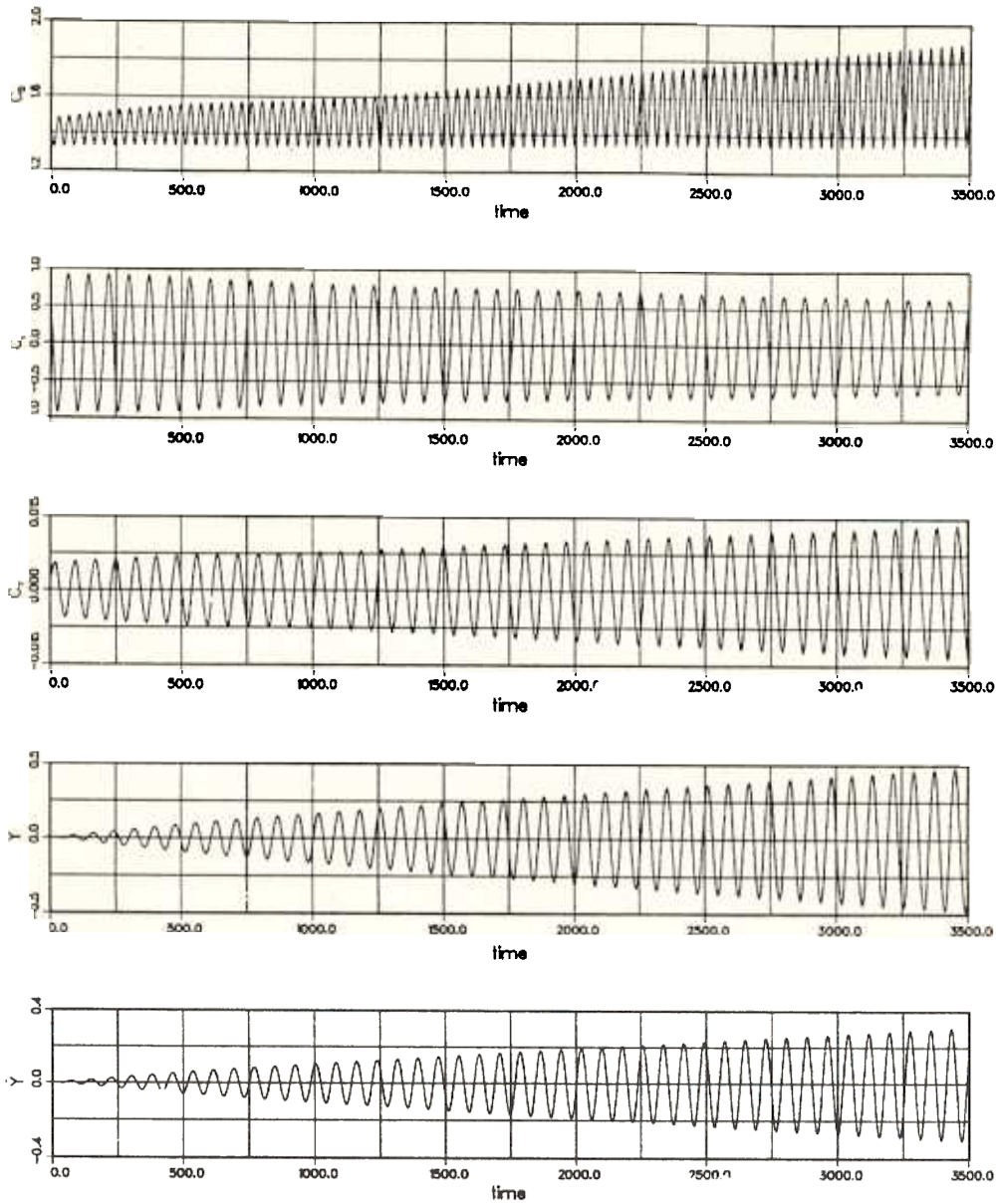

Figure 4. Flow past a vertically oscillating cylinder at Re = 324: initial time history of the lift, drag and torque coefficients and the normalized displacement and velocity of the cylinder

cylinder oscillates with an increasing amplitude. The drag and torque coefficients for the cylinder also increase while the lift coefficient shows a decreasing amplitude. It is interesting to note that both the mean and peak values of the drag coefficient increase with time, but the trough value remains almost constant. The quantities displayed in Figure 4 are shown in Figure 5 for a later stretch of time when the cylinder reaches a periodic oscillation amplitude of about one radius. The cylinder oscillates with its natural frequency, and so does the torque

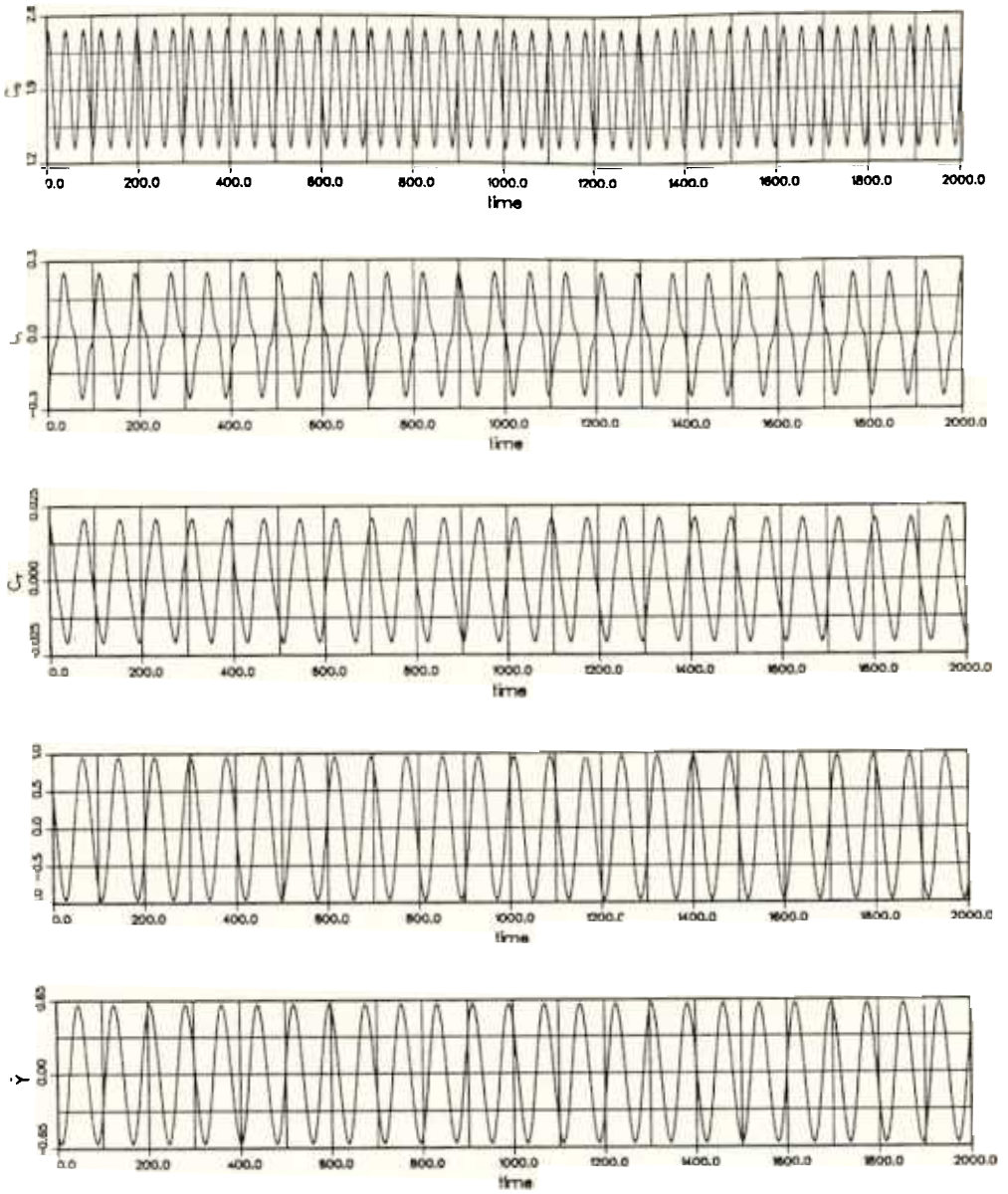

Figure 5. Flow past a vertically oscillating cylinder at Re = 324: later time history of the lift, drag and torque coefficients and the normalized displacement and velocity of the cylinder

coefficient; the drag coefficient oscillates with twice the natural frequency of the cylinder. The dominant frequency for the lift coefficient corresponds to the natural frequency of the cylinder. In addition, there is a very small component of the lift coefficient with thrice the frequency of the dominant one. Plates V and VI show a sequence of frames for the vorticity and stationary stream function during one period of the cylinder motion. In both figures, the first, third and last frames correspond to mean cylinder location, while the second and fourth frames correspond, respectively, to the lower and upper extreme positions of the cylinder.

For this case, in both parts of the animation (vorticity and stationary stream function), the first 500 time units show the unsteady flow past a fixed cylinder at Re 324. At the end of 500 time units the cylinder is released free in the vertical direction. In the animations, we can observe the classical Karman vortex street. During each cycle of cylinder motion two vortices are shed from the cylinder surface. The shedding alternates between the lower and the upper surfaces of the cylinder. It is also noticeable that the vortices shed from the upper surface of the cylinder rotate clockwise, while the vortices shed from the lower surface rotate counter-clockwise.

6. CONCLUDING REMARKS

The stabilized space–time formulation with Galerkin/least-squares stabilization has been reviewed for incompressible flows. Galerkin/least-squares stabilization leads to a formulation which is consistent. That is, the stabilization terms added to the Galerkin formulation of the problem vanish when an exact solution is substituted into the stabilized formulation. Consequently, this stabilization method introduces minimal excess diffusion, and therefore results in solutions with minimal loss of accuracy.

The formulation has been applied to certain unsteady, incompressible flow problems involving fixed and oscillating cylinders. To minimize the computational cost associated with these fairly large-scale problems, the CEBE iteration technique was employed to solve the equation systems resulting from the space–time finite element discretization.

Some interesting physical phenomena were observed as a result of these computations. While for flow past a fixed cylinder, the usual, asymmetric vortex shedding was observed, when the cylinder was subjected to horizontal oscillations of prescribed frequency and amplitude, symmetrical vortex shedding was observed instead. The case of vortex-induced vertical oscillations was also simulated. These oscillations result in an increase in the drag and torque coefficients and a decrease in the lift coefficient.

ACKNOWLEDGEMENT

This work was sponsored by the NASA-Johnson Space Center (under Grant NAG 9-499), the NSF (under Grant MSM-8796352) and the ALCOA foundation.

REFERENCES

1. T. J. R. Hughes, L. P. Franca and M. Mallet, 'A new finite element formulation for computational fluid dynamics: VI. Convergence analysis of the generalized SUPG formulation for linear time-dependent multi-dimensional advective-diffusive systems', *Computer Methods in Applied Mechanics and Engineering*, **63**, 97–112 (1987).
2. T. J. R. Hughes and G. M. Hulbert, 'Space–time finite element methods for elastodynamics: formulations and error estimates', *Computer Methods in Applied Mechanics and Engineering*, **66**, 339–363 (1988).
3. F. Shakib, 'Finite element analysis of the compressible Euler and Navier–Stokes equations', Ph.D. Thesis, Department of Mechanical Engineering, Stanford University, Stanford, California.
4. P. Hansbo and A. Szepessy, 'A velocity–pressure streamline diffusion finite element method for the incompressible Navier–Stokes equations', *Computer Methods in Applied Mechanics and Engineering*, **84**, 175–192 (1990).

5. T. E. Tezduyar, J. Liou and M. Behr, 'A new strategy for finite element computations involving moving boundaries and interfaces – the DSD/ST Procedure: I. The concept and the preliminary numerical tests', *University of Minnesota Supercomputer Institute Research Report*, UMSI 90/169, September 1990.
6. T. E. Tezduyar, J. Liou, M. Behr and S. Mittal, 'A new strategy for finite element computations involving moving boundaries and interfaces – the DSD/ST Procedure: II. Computation of free-surface flows, two-liquid flows, and flows with drifting cylinders', *University of Minnesota Supercomputer Institute Research Report*, UMSI 90/170, September 1990.
7. J. Liou and T. E. Tezduyar, 'Computation of compressible and incompressible flows with the clustered element-by-element method', *University of Minnesota Supercomputer Institute Research Report*, UMSI 90/215, October 1990.
8. Y. Saad and M. H. Schultz, 'GMRES: a generalized minimal residual algorithm for solving nonsymmetric linear systems', *SIAM J. Scient. Stat. Comput.*, 7, 856–869 (1986).
9. T. J. R. Hughes, I. Levit and J. Winget, 'An element-by-element solution algorithm for problems of structural and solid mechanics', *Computer Methods in Applied Mechanics and Engineering*, **36**, 241–254 (1983).
10. T. J. R. Hughes, J. Winget, I. Levit and T. E. Tezduyar, 'New alternating direction procedures in finite element analysis based upon EBE approximate factorizations', in S. N. Atlum and N. Perrone (eds.), *Recent Developments in Computer Methods for Nonlinear Solids and Mechanics*, Applied Mechanics Division, Vol. 54, ASME, New York, 75–109.
11. T. E. Tezduyar, R. Shih, S. Mittal and S. E. Ray, 'Incompressible flow computations with stabilized bilinear and linear equal-order-interpolation velocity–pressure elements', *University of Minnesota Supercomputer Institute Research Report*, UMSI 90/165, September 1990.
12. R. King, 'A review of vortex shedding research and its application', *Ocean Engineering*, **4**, 141–172 (1977, June).
13. T. Sarpkaya, 'Vortex-induced oscillations', *Journal of Applied Mechanics*, **46**, 241–258 (1979, June).
14. R. D. Blevins, *Flow-Induced Vibration*, 2nd edn., Van Nostrand Reinhold, New York, 1990.
15. O. M. Griffin and G. H. Koopmann, 'The vortex-excited lift and reaction forces on resonantly vibrating cylinders', *Journal of Sound and Vibration*, **54**(3), 435–448 (1979).

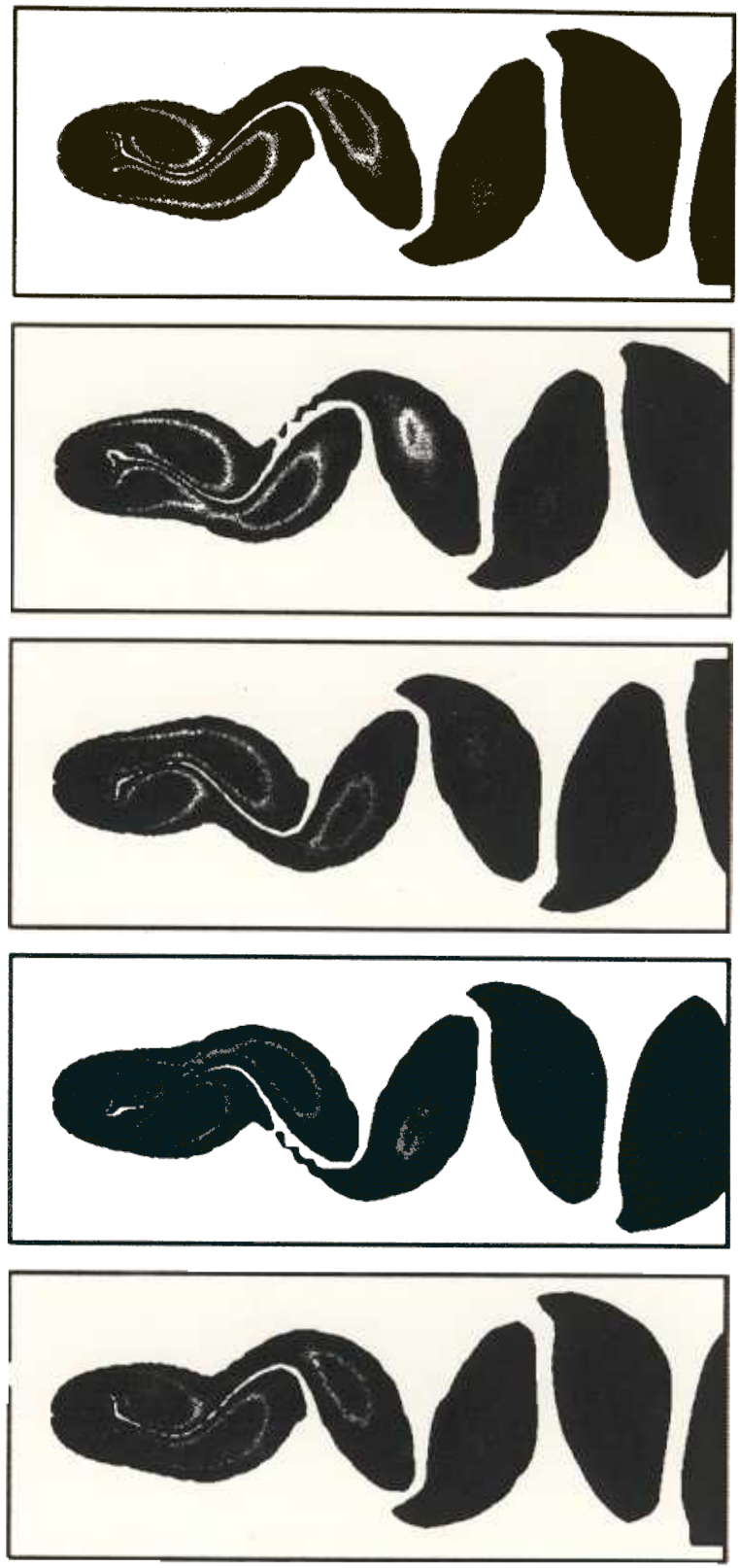

Plate I (Mittal *et al.*). Flow past a fixed cylinder at Re = 100: vorticity at various instants during one period of the lift coefficient

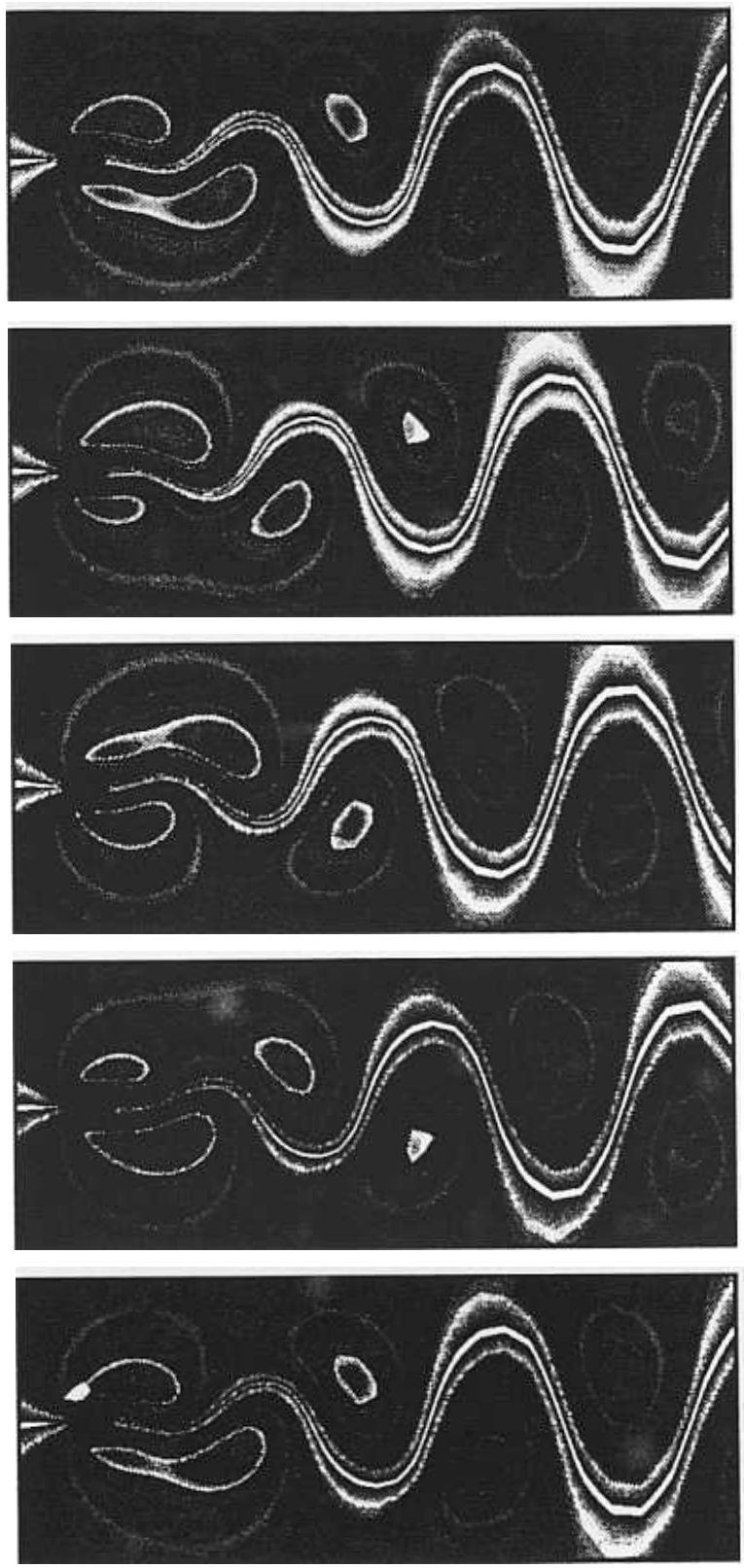

Plate II (Mittal *et al.*). Flow past a fixed cylinder at Re = 100: stationary stream function at various instants during one period of the lift coefficient

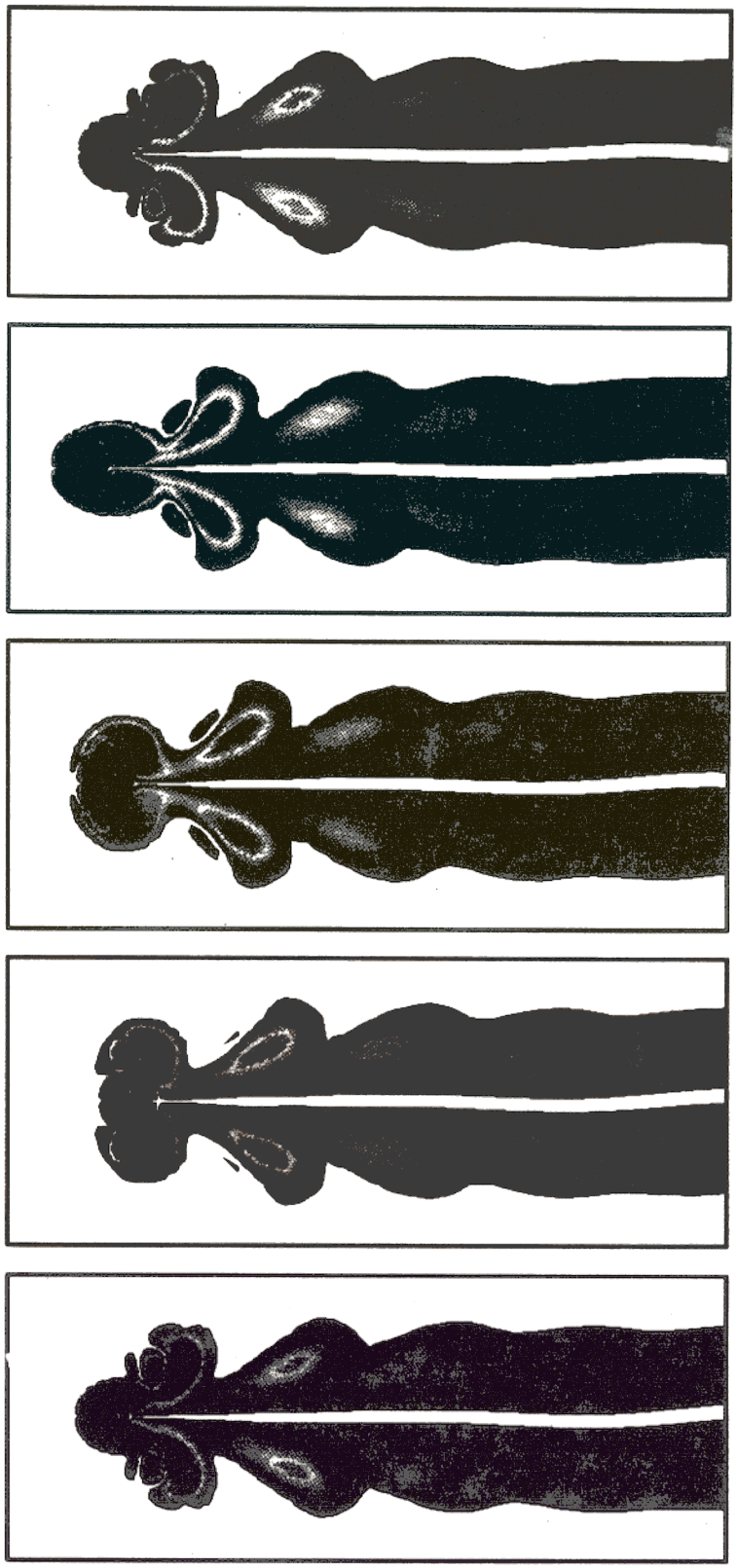

Plate III (Mittal *et al.*). Flow past a horizontally oscillating cylinder at Re = 100: vorticity at various instants during one period of the cylinder motion

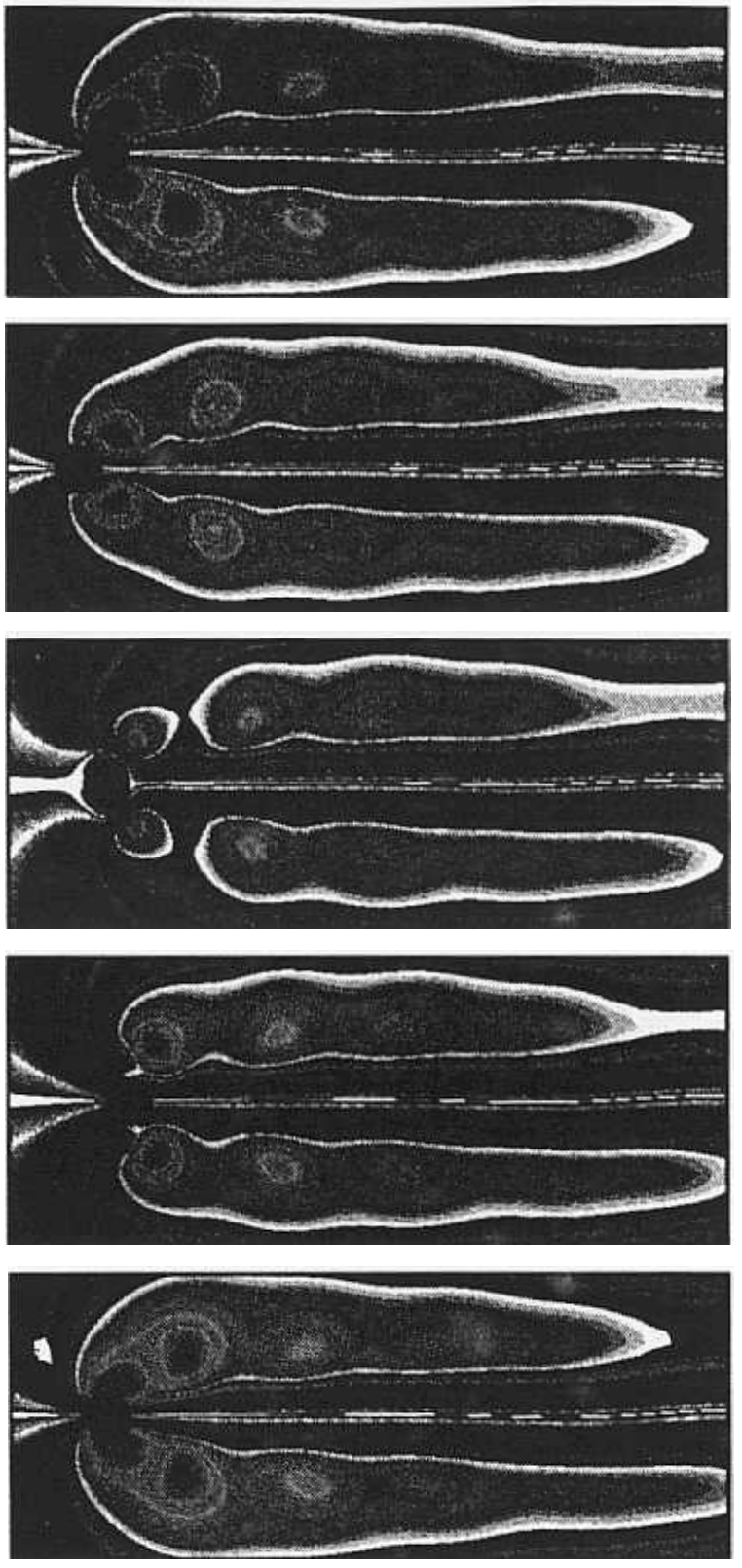

Plate IV (Mittal *et al.*). Flow past a horizontally oscillating cylinder at Re = 100: stationary stream function at various instants during one period of the cylinder motion

Plate V (Mittal *et al.*). Flow past a vertically oscillating cylinder at Re = 324: vorticity at various instants during one period of the cylinder motion

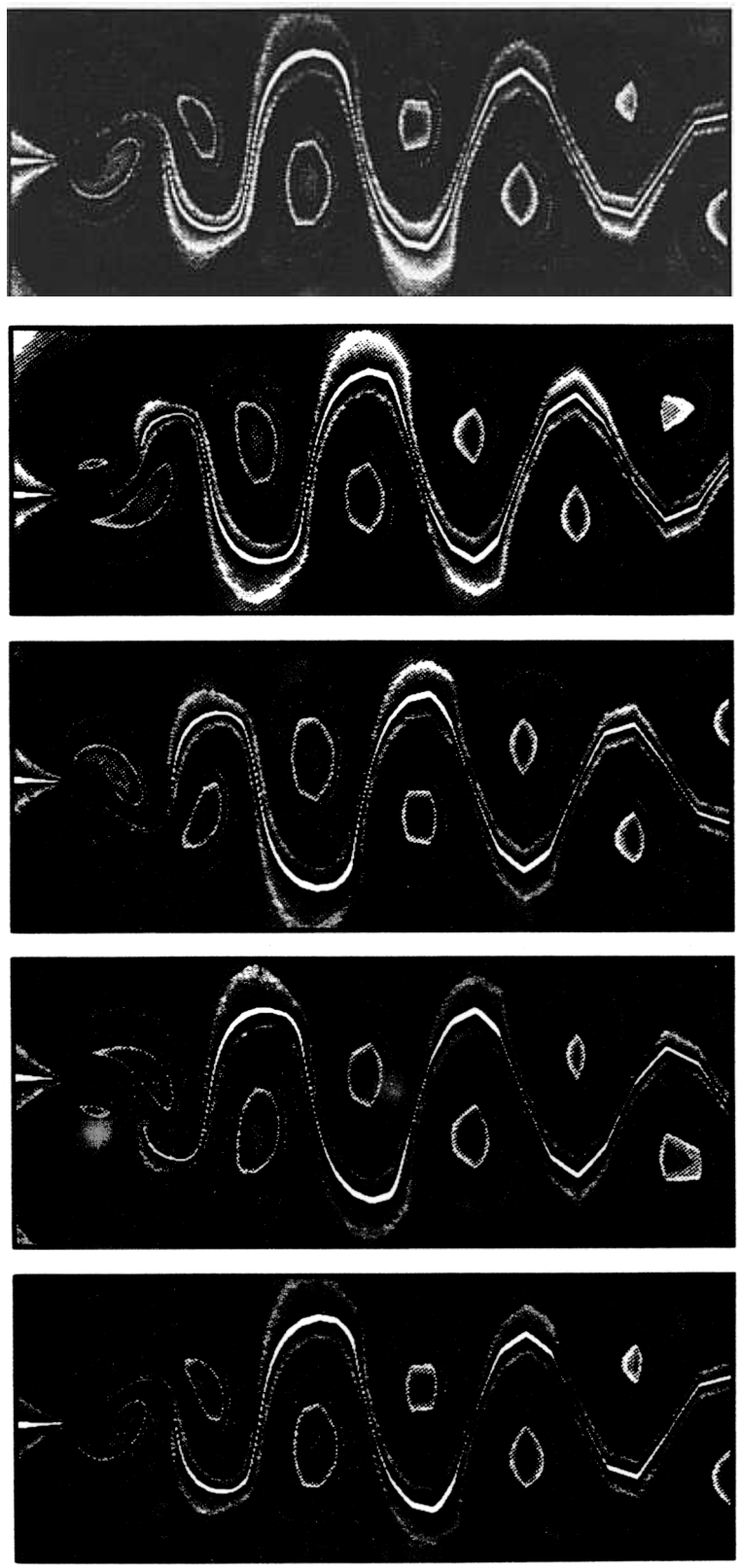

Plate VI (Mittal *et al.*). Flow past a vertically oscillating cylinder at Re = 324: stationary stream function at various instants during one period of the cylinder motion